Abstract

Fundamental $T(v_3)$ type high-J rovibrational fine structure is derived for a range of values of the Coriolis and $[2\times2]^4$ centrifugal constants. The theory of level clusters is developed further. Correlations are made between cluster states corresponding to well separated $P^{+,}$ Q^{0}, and R^{-} branches, and the opposite case in which $\Pi_{\pm}$ and Σ_0 labels are appropriate.

Centrifugal and Coriolis effects on level cluster patterns for $T(\nu_3)$ rovibrational bands in spherical top molecules

William G. Harter

Joint Institute for Laboratory Astrophysics, University of Colorado and National Bureau of Standards, Boulder, Colorado 80309

Chris W. Patterson and Harold W. Galbraith

Los Alamos Scientific Laboratory, Los Alamos, New Mexico 87545
(Received 2 March 1978)

Fundamental $T(\nu_3)$ type high-J rovibrational fine structure is derived for a range of values of the Coriolis and $[2\times2]^4$ centrifugal constants. The theory of level clusters is developed further. Correlations are made between cluster states corresponding to well separated P^+, Q^0, and R^- branches, and the opposite case in which $\Pi_\pm$ and Σ_0 labels are appropriate.

I. INTRODUCTION

The treatment of the complex fine structure in spherical top molecular spectra has become increasingly important due to interest in isotope separation[1] and new types of spectroscopy.[2] This article is one of a series[3-9] which treats a new approximate procedure for spectral analysis based on the theory of level cluster states. To put the present work in context, a brief introduction to the history of the problem and previous work is given.

The rotational fine structure in infrared spectra of methane (CH_4) was first resolved by Plyler *et al.*[10] in 1959. A theory for CH_4 spectra has been given by Louck, by Hecht, and by Moret-Bailly,[11] based partly on earlier work by Jahn[12] and others. However, until recently it has not been possible to study as much detail in the corresponding spectra of most other spherical top molecules. The small moment of inertia of CH_4 makes its spectral resolution easier than it is for the "heavy" tops. In addition the spectra of the heavy tops tend to be dominated by fine structure levels belonging to higher angular momentum J. [The most populated level has approximately $J=(kT/B)^{1/2}$.] The complexity and computational difficulty of the standard theory increases rapidly with J.

Recently, the advent of laser diode techniques[13] has increased spectral resolution by orders of magnitude. The application of these techniques has led to the identification of hundreds of lines in rovibrational spectra of SF_6, CF_4, and other heavy molecules.[14,15] Furthermore, these results have stimulated the development of a new theoretical approach which is more convenient for discussing high J states. The new approach is based upon the observation of energy level "clustering" within the fine structure spectrum of SF_6 and in computer model eigenvalue distributions.[16]

Clustering had been noticed earlier by Lea, Leask, and Wolf[17] in crystal field splitting computations, and by Dorney and Watson[18] in computer diagonalization of model CH_4 Hamiltonians. A classical explanation given by Dorney and Watson tells why the most clusters have sixfold or else eightfold degeneracy. One imagines that a tetrahedral or octahedral top undergoes stable classical rotation around one of its six fourfold symmetry axes, or else around one of its eight threefold axes.

A quantum model developed by Harter and Patterson[3-5] explains the structure of various types of clusters by making an analogy with band theory in solids.[6] The form of cluster splitting is predicted by a theory of axis tunneling or tumbling of the molecule between different internal rotation axes. A simple symmetry analysis of induced representations (IR) tells which cubic or tetrahedral IR show up in each cluster. For example the four types of fourfold clusters (0_4), (1_4), (2_4), and (3_4) split into cubic IR as follows:

$$\begin{aligned}(c_4)=(0_4)&=A_1+T_1+E\ ,\\ (1_4)&=T_1+T_2\ ,\\ (2_4)&=A_2+T_2+E\ ,\\ (3_4)&=T_1+T_2\ .\end{aligned}\tag{1a}$$

Each cluster state $|(c_4)\rangle$ will, in general, be a combination of angular momentum states $|r_n^J\rangle$ for which the internal component (n) on the molecular fourfold axis satisfies

$$n=c \bmod 4\ .\tag{1b}$$

Similarly, three types of threefold clusters (0_3), (1_3), and (2_3) split as follows:

$$\begin{aligned}(c_3)=(0_3)&=A_1+T_1+T_2+A_2\ ,\\ (1_3)&=T_1+E+T_2\ ,\\ (2_3)&=T_1+E+T_2\ .\end{aligned}\tag{2a}$$

Each cluster state $|(c_3)\rangle$ involves combinations of threefold axial momentum (n) satisfying

$$n=c \bmod 3\ .\tag{2b}$$

By making cluster states the starting point of spherical top theory one can greatly simplify the analysis. Roughly speaking a gas of tetrahedral or octahedral molecules can be thought of as being composed of two different species of axially symmetric molecules. One species is rotating around fourfold axes and is centrifugally distorted into C_4 symmetry, while the other species is rotating about threefold axes and is distorted into C_3 symmetry.

Within each species there are subspecies belonging to each type of cluster, and depending on how the hyperfine splitting compares with the cluster splitting, there may

 0021-9606/78/6911-4896$01.00

also be octahedral subsubspecies.[7] Using a cluster analysis it was possible for the first time to derive surprisingly simple and accurate algebraic formulas for P, Q, and R branches of the $T_{1u}(\nu_3)$ bands of SF_6 around 948 cm^{-1} and the $F_2(\nu_3)$ bands of CF_4 around 631 cm^{-1}.[8] One set of formulas gives fourfold cluster positions while another set gives threefold clusters, and together they predict most of the rovibronic spectrum correctly to within the Doppler width of observed lines. The formulas are constructed using a perturbation theory in which one assumes that the Coriolis parameter $B\zeta$ is much larger than the tensor centrifugal parameters g or h. This is the case for $SF_6(B\zeta = 6.28\times10^{-2}$, $g = -2.46\times10^{-5}$, $h = -5\times10^{-10})$ and for $CF_4(B\zeta = -6.7\times10^{-2}$, $g = -2.65\times10^{-5}$, $h = -1.26\times10^{-7})$. (See Refs. 19a and 19b).

In Sec. III of this paper, the (ν_3) cluster spectrum will be examined for cases in which $B\zeta$ is zero or small compared to the principal centrifugal parameter g (h will be assumed zero). A model rovibrational Hamiltonian including the important centrifugal and Coriolis parts will be represented in two different but equivalent bases. The first basis (Sec. II) is a cluster adaptation of a basis used by Hecht,[11] which we call the weak-coupling (WC) basis, and the second basis (Sec. III) will be a different one which we have named the Born–Oppenheimer approximation (BOA) basis.[7] In the WC basis the nuclear rotor momentum quantum number N (N is labeled R in most other works) is a good quantum number, and this basis is more appropriate for small $g/B\zeta$. In the BOA basis the internal vibrational momentum component Λ on the axis of rotation will be a good quantum number. As we will see, BOA bases are more appropriate for large $g/B\zeta$. In either basis, the cluster labels (c_3) or (c_4) and total momentum $\langle J\rangle = \langle N + l\rangle$ will be good quantum labels.

In a previous article[9] a BOA basis was used to derive rovibrational cluster patterns for doubly-degenerate $E(\nu_2)$ type vibrations (E vibrations have no first order Coriolis type interactions), and so the present work is a natural extension to triply-degenerate T or $F(\nu_{3,4})$ vibrations for cases of very high J and/or low $|g/B\zeta|$. With so many different types of overtone[19c] and combination bands being studied in many new types of spectroscopy, it is important to see how energy levels and clusters correlate between different extremes in the range of the most important centrifugal and Coriolis parameters. In addition, we expect that the BOA bases will be very useful for unraveling electronic and vibronic bands in the future.

II. CORIOLIS AND $[2\times2]^4$ CENTRIFUGAL HAMILTONIAN IN WC CLUSTER BASIS

Consider the following model rovibrational Hamiltonian

$$H_M = \omega + B\bar{J}^2 - 2B\zeta\bar{J}\cdot\bar{l} + t_{224}[\bar{V}^2(\mathrm{rot})\times\bar{V}^2(\mathrm{vib})]^4 , \quad (3a)$$

where our centrifugal constant is $g = -(t_{224}/2)\sqrt{12/7}$. The Coriolis part can be written as,

$$-2B\zeta\bar{J}\cdot\bar{l} = -B\zeta[J^2 - N^2 + l^2] , \quad (3b)$$

in terms of squares of total momentum $(J = N + l)$, nuclear rotor momentum (N) and vibrational momentum (l). Depending on whether one uses threefold or fourfold axis of quantization, the centrifugal operator is represented one of two ways:

$$[\bar{V}^2(\mathrm{rot})\times\bar{V}^2(\mathrm{vib})]^4 = \begin{cases} -\frac{2}{3}\{\sqrt{70}\,[\bar{V}^2\times\bar{V}^2]^4_0 - 10([\bar{V}^2\times\bar{V}^2]^4_3 - [\bar{V}^2\times\bar{V}^2]^4_{-3})(\text{for threefold axes})\} & (3c) \\ \{\sqrt{70}\,[\bar{V}^2\times\bar{V}^2]^4_0 + 5([\bar{V}^2\times\bar{V}^2]^4_4 + [\bar{V}^2\times\bar{V}^2]^4_{-4})(\text{for fourfold axes}\} , & (3d) \end{cases}$$

in terms of tensor products,

$$[\bar{V}^{k_1}\times\bar{V}^{k_2}]^K_Q = \sum_{q_1q_2} C^{k_1k_2K}_{q_1q_2Q}\bar{V}^{k_1}_{q_1}(\mathrm{rot})\bar{V}^{k_2}_{q_2}(\mathrm{vib}) , \quad (3e)$$

of rotational and vibrational unit tensor operators to be defined in Sec. III. We shall not discuss other tensor operators such as $h[\bar{V}^3\times\bar{V}^1]$ or higher order tensors considered by Hecht,[11] since our treatment is only meant to illustrate the generic structure of the spectrum.

In the absence of centrifugal distortion ($g = 0$) the level spectrum for $(l = 1)$ is a comparatively simple function of the Coriolis parameter ζ, as shown by Fig. 1. Since the centrifugal operator is an internal or body-defined operator, it can couple only those states with the same total momentum J. The three levels of rotor momentum $N = J - 1$, J, and $J + 1$ which have the same J are degenerate when $B\zeta = 0$. Then a small centrifugal operator can effectively mix the three states and thus spoil N as a quantum number.

One may view the "Coriolis splitting" shown in Fig. 1 in two ways. On the one hand it can be imagined that vibrational momentum $(l = 1)$ is added to a given rotor momentum N to make three components $J = N + 1$, N, and $N - 1$ which split away from each N-labeled point on the left side of Fig. 1. On the other hand one can imagine that $(l = 1)$ is subtracted from a given J state to make three N levels of nuclear rotor momentum $N = J - 1$, $N = J$, and $N = J + 1$ which split off from each J-labeled point on the right side of Fig. 1 as ζ becomes nonzero.

Using either viewpoint, one makes virtually the same wavefunctions of definite l, N, J, and body axis component of momentum n. (n is labeled K_R or K_c in most other works.) By coupling l and N one defines the WC wave function,

$$\langle|[lN]^J_M(n)\rangle \equiv \sum_{\lambda m} C^{lNJ}_{\lambda mM}\phi^l_\lambda(\mathrm{vib})r^N_{mn}(\mathrm{rot}) , \quad (4)$$

where $\phi^l_\lambda(\mathrm{vib})$ is an angular vibration function defined in laboratory fixed coordinates $\{xyz\}$, and $r^N_{mn}(\mathrm{rot})$ is a rotor wavefunction,

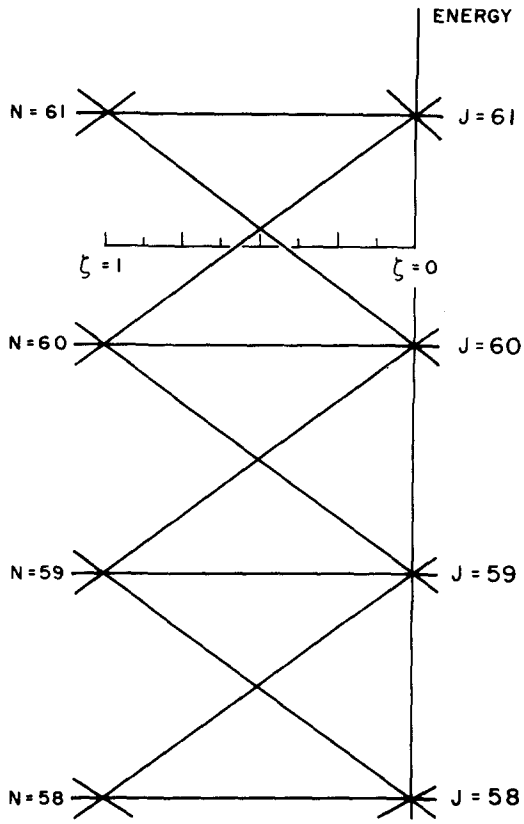

FIG. 1. ($l=1$) Coriolis energy level trajectories for zero centrifugal splitting.

$$r^N_{mn}(\mathrm{rot}) = \mathfrak{D}^N_{mn}(\alpha\beta\gamma)^*\sqrt{[N]}\,, \tag{5}$$

where $[N]\equiv 2N+1$, and $\mathfrak{D}^N_{mn}$ is an irreducible rotational matrix component. The wave function in Eq. (4) can just as well be written in terms of vibration functions $\Phi^l_\Lambda(\overline{\mathrm{vib}})$ defined in the molecule-fixed coordinates $\{\bar{x}\,\bar{y}\,\bar{z}\}$,

$$\phi^l_\Lambda(\overline{\mathrm{vib}}) = \sum_\lambda \phi^l_\lambda(\mathrm{vib})\mathfrak{D}^l_{\lambda\Lambda}(\alpha\beta\gamma)\,. \tag{6}$$

Inserting the inverse,

$$\phi^l_\lambda(\mathrm{vib}) = \sum_\Lambda \phi^l_\Lambda(\overline{\mathrm{vib}})\mathfrak{D}^l_{\lambda\Lambda}(\alpha\beta\gamma)^*\,,$$

into Eq. (4) and using standard Clebsch–Gordon coefficient relations,[7,20] we obtain the following expression:

$$\begin{aligned}\langle|[lN](n)^J_M\rangle &= \sum_\Lambda C^{lnJ}_{\Lambda nK}\sqrt{\frac{[N]}{[J]}}\,\phi^l_\Lambda(\overline{\mathrm{vib}})r^J_{MK=n+\Lambda}\,,\\ &= (-1)^{N-J}\sum_\Lambda C^{lJN}_{\Lambda Kn}(-1)^\Lambda\phi^l_{-\Lambda}(\overline{\mathrm{vib}})r^J_{MK=n-\Lambda}\,,\\ &= (-1)^{N-J}\sum_\Lambda C^{lJN}_{\Lambda Kn}\phi^{l*}_\Lambda(\overline{\mathrm{vib}})r^J_{MK=n-\Lambda}\,.\end{aligned} \tag{7}$$

This differs only by the phase $(-1)^{N-J}$ from the wavefunction,

$$\begin{aligned}\langle|[lJ](M)^N_n\rangle &\equiv (-1)^{N-J}\langle|[lN](n)^J_M\rangle\,,\\ &= \sum_\Lambda C^{lJN}_{\Lambda Kn}\phi^{l*}_\Lambda(\overline{\mathrm{vib}})r^J_{MK=n-\Lambda}\,,\end{aligned} \tag{8}$$

in which l is "subtracted" from J to give N. The $\langle|[lJ]N\rangle$ wavefunction is in a form for which matrix elements of internal operators $[V^{k_1}(\overline{\mathrm{vib}})\times V^{k_2}(\overline{\mathrm{rot}})]^K_Q$ can be expressed in terms of coupling and 9-j recoupling coefficients.

Following Hecht[11] one obtains,

$$\begin{aligned}&\langle[l'J']^{N'}_{n'}|[V^{k_1}(\overline{\mathrm{vib}})\times V^{k_2}(\overline{\mathrm{rot}})]^K_Q|[lJ]^N_n\rangle\\ &\quad = C^{NKN'}_{nQn'}\langle[l'J']N'\|[k_1k_2]K\|[lJ]N\rangle/\sqrt{[N']}\,,\end{aligned} \tag{9a}$$

where the reduced matrix element is given by,

$$\begin{aligned}&\langle[l'J']N'\|[k_1k_2]K\|[lJ]N\rangle = ([N'][N][K])^{1/2}\\ &\times\begin{Bmatrix} l' & l & k_1\\ J' & J & k_2\\ N' & N & K\end{Bmatrix}\langle l'\|k_1\|l\rangle_{\mathrm{vib}}\langle J'\|k_2\|J\rangle_{\mathrm{rot}}\,.\end{aligned} \tag{9b}$$

For the centrifugal operator of interest one needs,

$$\begin{aligned}&\langle[1J]N'\|[2\ 2]4\|[1J]N\rangle = 3([N'][N])^{1/2}\\ &\times\begin{Bmatrix} 1 & 1 & 2\\ J & J & 2\\ N' & N & 4\end{Bmatrix}\langle 1\|2\|1\rangle_{\mathrm{vib}}\langle J\|2\|J\rangle_{\mathrm{rot}}\,,\end{aligned} \tag{10}$$

where the 9-j coefficient reduces to,

$$\begin{Bmatrix} 1 & 1 & 2\\ J & J & 2\\ N' & N & 4\end{Bmatrix} = \begin{Bmatrix} N' & J & 3\\ 1 & 4 & N\end{Bmatrix}\begin{Bmatrix} J & J & 2\\ 1 & 3 & N'\end{Bmatrix}\left(\frac{7}{5}\right)^{1/2}\,, \tag{11}$$

and the reduced matrix elements are,

$$\begin{aligned}&\langle 1\|2\|1\rangle_{\mathrm{vib}} = -\sqrt{5}\,,\\ &\langle J\|2\|J\rangle_{\mathrm{rot}} = [(2J+3)(2J+2)2J(2J-1)/24)]^{1/2}\,.\end{aligned} \tag{12}$$

Finally, by combining algebraic expressions for all the angular coefficients we obtain the matrix elements listed in Tables I and II for the Hamiltonian in Eq. (3a), where we define $g\equiv -(t_{224}/2)\sqrt{12/7}$.

As long as $B\zeta \gg g$ and J has intermediate values, the diagonal matrix elements give the energy level clusters fairly accurately,[8] and this is called the first-order dominant approximation. Then each cluster level is labeled by a definite core momentum component (n) as well as the cluster label (c_4) determined by Eq. (1b), the total rotor momentum N, and of course J. Components $N=J+1$, $N=J$, and $N=J-1$ are associated with "allowed" $P^+(N)$, $Q^0(N)$, and $R^-(N)$ transitions or branches, respectively, of the infrared spectrum. (One should note that if N is a "good" quantum number, then transitions between states of different N, due to externally applied radiation, are forbidden, as explained in Ref. 7.) As total momentum J or $g/B\zeta$ increases the coupling increases between states of different N and n due to off-diagonal $N\pm1$ and $n\pm4$ components in Table I.

A similar matrix exists for rotational states involving the threefold axis (see Table II). The main difference is that states with threefold component n couple with those having $n\pm3$ and correspond to c_3 clusters as given by Eqs. (2a) and (2b). The diagonal components and those relating states of the same n are equal to the corresponding fourfold components multiplied by $(-2/3)$.

III. CORIOLIS AND $[2\times2]^4$ CENTRIFUGAL HAMILTONIAN IN BOA CLUSTER BASIS

It is convenient to rewrite the centrifugal operator in Eq. (3) in terms of angular momentum operators and vi-

TABLE I. Upper diagonal of fourfold centrifugal matrix in WC cluster basis [$g=(12/7)^{1/2}$ is chosen]. [a]

n			$n-4$		
$\|N=J+1\rangle$	$\|N=J\rangle$	$\|N=J-1\rangle$	$\|N=J+1\rangle$	$\|N=J\rangle$	$\|N=J-1\rangle$
$\frac{x^{J+1}(n+4)}{(2J+2)(2J+1)}$	$\frac{y^{J}(n)}{[2J(2J+1)]^{1/2}}$	$z(n)$			
$\frac{-y^{J}(n+4)}{[2J(2J+1)]^{1/2}}$	$\frac{-2x^{J}(n+4)}{2J(2J+2)}$	$\frac{-y^{J-1}(n)}{[(2J+2)(2J+1)]^{1/2}}$			
$z(n+4)$	$\frac{y^{J-1}(n+4)}{[(2J+1)(2J+2)]^{1/2}}$	$\frac{x^{J-1}(n+4)}{2J(2J+1)}$			
$\frac{a^{J+1}(n)}{(2J+2)(2J+1)}$	$\frac{b^{J}(n)}{[J(2J+1)]^{1/2}}$	$-c(n)$	$\frac{x^{J+1}(n)}{(2J+2)(2J+1)}$	$\frac{y^{J}(4-n)}{[2J(2J+1)]^{1/2}}$	$z(4-n)$
	$\frac{-2a^{J}(n)}{2J(2J+2)}$	$\frac{-b^{J-1}(n)}{[(J+1)(2J+1)]^{1/2}}$	$\frac{-y^{J}(n)}{[2J(2J+1)]^{1/2}}$	$\frac{-2x^{J}(n)}{2J(2J+2)}$	$\frac{-y^{J-1}(4-n)}{[(2J+2)(2J+1)]^{1/2}}$
		$\frac{a^{J-1}(n)}{2J(2J+1)}$	$z(n)$	$\frac{y^{J-1}(n)}{[(2J+1)(2J+2)]^{1/2}}$	$\frac{x^{J-1}(n)}{2J(2J+1)}$
			$\frac{a^{J+1}(n-4)}{(2J+2)(2J+1)}$	$\frac{b^{J}(n-4)}{[J(2J+1)]^{1/2}}$	$-c(n-4)$
				$\frac{-2a^{J}(n-4)}{2J(2J+2)}$	$\frac{-b^{J-1}(n-4)}{[(J+1)(2J+1)]^{1/2}}$
					$\frac{a^{J-1}(n-4)}{2J(2J+1)}$

[a]Values of components are given by

$$a^J(n)=6(J+2)(J+1)J(J-1)-10n^2(6J^2+6J-5)+70n^4,\quad b^J(n)=\frac{5n(3J^2+6J-2-7n^2)[(J+n+1)(J-n+1)]^{1/2}}{(J+1)},$$

$$c^J(n)=\frac{5(J^2+J-2-7n^2)[2(J+n+1)(J+n)(J-n+1)(J-n)]^{1/2}}{(2J+1)[J(2J+2)]^{1/2}},$$

$$x^J(n)=5[(J+n)(J+n-1)(J+n-2)(J+n-3)(J+n-4)(J-n+3)(J-n+2)(J-n+1)]^{1/2},$$

$$y^J(n)=\frac{5[2(J+n)(J+n-1)(J+n-2)(J-n+5)(J-n+4)(J-n+3)(J-n+2)(J-n+1)]^{1/2}}{(2J+2)},$$

$$z(n)=\frac{5[(J+n-1)(J+n-2)(J-n+5)(J-n+4)(J-n+3)(J-n+2)(J-n+1)(J-n)]^{1/2}}{(2J+1)[2J(2J+2)]^{1/2}}.$$

bration creation–destruction operators. The three octahedral $T_{1u}(\nu_3)$ type base functions correspond to components $\bar{x}$, $\bar{y}$, and $\bar{z}$. However, for angular momentum analysis it is convenient to deal with the following combinations:

$$\begin{aligned} \mathcal{Y}_1^{T_1 \text{ or } {}^1F_2} &= Y_1^1 \sim -(x+iy)/\sqrt{2}\ , \\ \mathcal{Y}_0 &= Y_0^1 \sim z\ , \\ \mathcal{Y}_{-1} &= Y_{-1}^1 \sim (x-iy)/\sqrt{2}\ , \end{aligned} \tag{13}$$

and we shall define angular creation operators in an analogous fashion;

$$\begin{aligned} a_1^\dagger &= -(a_x+ia_x)/\sqrt{2}\ , \\ a_0^\dagger &= a_z\ , \\ a_{-1}^\dagger &= (a_x-ia_y)/\sqrt{2}\ . \end{aligned} \tag{14}$$

However, note that conjugate destruction operators $(-1)^m a_m$ transform like creation operators $a_m^\dagger$, i.e., $(-a_{-1}, a_0, -a_1)$ forms a T_{1u} basis. Therefore the vibrational tensor is computed from

$$V_q^2(\overline{\text{vib}}) = \sum_{a,b} C_{abq}^{112} a_a^\dagger a_{-b}(-1)^b\ , \tag{15}$$

to give

$$\begin{aligned} V_{\pm 2}^2(\overline{\text{vib}}) &= a_{\pm 1}^\dagger a_{\mp 1}\ , \\ V_{\pm 1}^2 &= (a_0^\dagger a_\mp - a_{\pm 1}^\dagger a_0)/\sqrt{2}\ , \\ V_0^2 &= (a_1^\dagger a_1 - 2a_0^\dagger a_0 + a_{-1}^\dagger a_{-1})/\sqrt{6}\ . \end{aligned} \tag{16}$$

Similarly, the rotational part,

$$V_q^2(\overline{\text{rot}}) \equiv T_q^2\ ,$$

can be built from quadratic products of angular momentum operators,

$$\begin{aligned} J_1^1 &\equiv -(J_x+iJ_y)/\sqrt{2} \equiv -J_+/\sqrt{2}\ , \\ J_0^1 &\equiv J_z\ , \\ J_{-1}^1 &= (J_x-iJ_y)/\sqrt{2} \equiv J_-/\sqrt{2}\ . \end{aligned} \tag{17}$$

Using Eq. (3e) to assemble the two parts we have,

$$\begin{aligned} [V^2\times V^2]_0^4 &= \sqrt{\tfrac{1}{70}}(T_2^2V_{-2}^2 + T_{-2}^2V_2^2) \\ &\quad + \sqrt{\tfrac{8}{35}}(T_1^2V_{-1}^2 + T_{-1}^2V_1^2) + \sqrt{\tfrac{18}{35}}T_0^2V_0^2\ , \\ [V^2\times V^2]_{\pm 3}^4 &= \sqrt{\tfrac{1}{2}}\,T_{\pm 2}^2V_{\pm 1}^2 + \sqrt{\tfrac{1}{2}}\,T_{\pm 1}^2V_{\pm 2}^2\ , \\ [V^2\times V^2]_{\pm 4}^4 &= T_{\pm 2}^2V_{\pm 2}^2\ . \end{aligned} \tag{18}$$

The desired expressions for threefold and fourfold quantized centrifugal operators are found to be, using Eqs. (3c) and (3d), respectively,

$$[V^2\times V^2]^4=(\tfrac{2}{3})\{T_2^2(5a_0^\dagger a_{-1}-5a_1^\dagger a_0-a_{-1}^\dagger a_1)+T_{-2}^2(5a_{-1}^\dagger a_0-5a_0^\dagger a_1-a_1^\dagger a_{-1})+\sqrt{2}\,[T_{-1}^2(2a_1^\dagger a_0-2a_0^\dagger a_{-1}-5a_{-1}^\dagger a_1)$$
$$+T_1^2(2a_{-1}^\dagger a_0-a_0^\dagger a_1+5a_1^\dagger a_{-1})]-\sqrt{6}\,T_0^2(a_1^\dagger a_1-2a_0^\dagger a_0+a_{-1}^\dagger a_{-1})\}\ \text{(threefold axis)}\ , \tag{19a}$$

and

$$[V^2\times V^2]^4=\{T_2^2(a_{-1}^\dagger a_1+5a_1^\dagger a_{-1})+T_{-2}^2(a_1^\dagger a_{-1}+5a_{-1}^\dagger a_1)$$
$$+2\sqrt{2}\,[T_1^2(a_0^\dagger a_1-a_{-1}^\dagger a_0)+T_{-1}^2(a_0^\dagger a_{-1}-a_1^\dagger a_0)]+\sqrt{6}\,T_0^2(a_1^\dagger a_1-2a_0^\dagger a_0+a_{-1}^\dagger a_{-1})\}\ \text{(fourfold axis)}\ . \tag{19b}$$

The BOA states will be used as a basis to represent $[V^2\times V^2]^4$. The BOA wavefunction is defined by[7,20]

$$\langle|\,|(\text{BOA})\Lambda n_M^J\rangle=\phi_\Lambda^l(\overline{\text{vib}})r_{MK=\Lambda+n}^J\ , \tag{20}$$

for the $(l=1)$ vibrations being considered, the component Λ on the internal rotation axis can have the values $\Lambda=1$, 0, and -1, and the corresponding BOA states will be labeled Π_+, Σ_0, and Π_-, respectively. From Eq. (7) we see that the WC wavefunction is related by the following unitary transformation

$$\langle|\,|[lN](n)_M^J\rangle=\sum_\Lambda C_{\Lambda nK}^{lNJ}\sqrt{\frac{[N]}{[J]}}\langle|\,|(\text{BOA})\Lambda(n)_M^J\rangle\ ,$$
$$\langle|\,|(\text{BOA})\Lambda(n)_M^J\rangle=\sum_N C_{\Lambda nK}^{lNJ}\sqrt{\frac{[N]}{[J]}}\langle|\,|[lN](n)_M^J\rangle\ . \tag{21}$$

Clearly, N is not a good quantum number for BOA bases, and neither Λ nor $K=n+\Lambda$ are good for WC bases. The transformation matrix in Eq. (21) is written out in Table III.

It is probably easier to calculate the Hamiltonian matrix directly in the BOA basis rather than transforming Tables I and II with Table III. The matrix elements of Eq. (19) are found using the standard rules for $a^\dagger$, a operators on their vibration wave functions $\phi_\Lambda(\text{vib})$, and the following "reverse angular momentum rules" on the rotational wavefunctions,

$$\langle r_{MK'=K+q}^J|\,T_{-q}^2\,|r_{MK}^J\rangle=C_{qKK'}^{2JJ}\langle J\,\|2\,\|J\rangle/\sqrt{[J]}$$
$$=\begin{pmatrix}J & 2 & J\\ K & q & -K'\end{pmatrix}(-1)^{J-K'}\langle J\,\|2\,\|J\rangle\ . \tag{22}$$

The reverse rules make it so the Hamiltonian in Eqs. (19a) or (19b) will couple the states belonging to (n) only to those belonging to $(n \bmod 3)$ or $(n \bmod 4)$, respectively.

TABLE II. Upper diagonal of threefold centrifugal matrix in WC cluster basis [$g=(12/7)^{1/2}$ is chosen].[a]

		n	$n-3$		
$\lvert N=J+1\rangle$	$\lvert N=J\rangle$	$\lvert N=J-1\rangle$	$\lvert N=J+1\rangle$	$\lvert N=J\rangle$	$\lvert N=J-1\rangle$
$\frac{2}{3}t^{J+1}(n+3)/(2J+2)(2J+1)$	$\frac{2}{3}u^J(n)/[2J(2J+1)]^{1/2}$	$-\frac{2}{3}v(n)$			
$-\frac{2}{3}u^J(n+3)/[2J(2J+1)]^{1/2}$	$-\frac{4}{3}t^J(n+3)/2J(2J+2)$	$-\frac{2}{3}u^{J-1}(n)/[(2J+1)(2J+2)]^{1/2}$			
$\frac{2}{3}v(n+3)$	$\frac{2}{3}u^{J-1}(n+3)/[(2J+1)(2J+2)]^{1/2}$	$\frac{2}{3}t^{J-1}(n+3)/2J(2J+1)$			
$-\frac{2}{3}a^{J+1}(n)/(2J+2)(2J+1)$	$-\frac{2}{3}b^J(n)/[J(2J+1)]^{1/2}$	$\frac{2}{3}c(n)$	$\frac{2}{3}t^{J+1}(n)/(2J+2)(2J+1)$	$\frac{2}{3}u^J(3-n)/[2J(2J+1)]^{1/2}$	$-\frac{2}{3}v(3-n)$
	$\frac{4}{3}a^J(n)/2J(2J+2)$	$\frac{2}{3}b^{J-1}(n)/[(J+1)(2J+1)]^{1/2}$	$-\frac{2}{3}u^J(n)/[2J(2J+1)]^{1/2}$	$-\frac{4}{3}t^J(n)/2J(2J+2)$	$-\frac{2}{3}u^{J-1}(3-n)/[(2J+1)(2J+2)]^{1/2}$
		$-\frac{2}{3}a^{J-1}(n)/2J(2J+1)$	$\frac{2}{3}v(n)$	$\frac{2}{3}u^{J-1}(u)/[(2J+1)(2J+2)]^{1/2}$	$\frac{2}{3}t^{J-1}(n)/2J(2J+1)$
			$-\frac{2}{3}a^{J+1}(n-3)/(2J+2)(2J+1)$	$-\frac{2}{3}b^J(n-3)/[J(2J+1)]^{1/2}$	$\frac{2}{3}c(n-3)$
				$\frac{4}{3}a^J(n-3)/2J(2J+2)$	$\frac{2}{3}b^{J-1}(n-3)/[(J+1)(2J+1)]^{1/2}$
					$-\frac{2}{3}a^{J-1}(n-3)/2J(2J+1)$

[a]Values of components are given by

$$t^J(n)=10(2n-3)[2(J+n)(J+n-1)(J+n-2)(J-n+3)(J-n+2)(J-n+1)]^{1/2},$$
$$u^J(n)=\frac{5(J+4n-5)[(J+n)(J+n-1)(J-n+4)(J-n+3)(J-n+2)(J-n+1)]^{1/2}}{J+1}\ ,$$
$$v(n)=\frac{5(2J+4n-5)[(J+n-1)(J-n+4)(J-n+3)(J-n+2)(J-n+1)(J-n)]^{1/2}}{(2J+1)[J(2J+2)]^{1/2}}\ .$$

(a, b, and c components are given under Table I.)

TABLE III. n-block of transformation matrix between WC and BOA cluster basis.

	$\|N=J-1\rangle$	$\|N=J\rangle$	$\|N=J+1\rangle$
$\langle \Pi_{(\Lambda=+1)} \|$ $(K=n+1)$	$\left[\frac{(J+n)(J+n+1)}{2J(2J+1)}\right]^{1/2}$	$\left[\frac{(J+n+1)(J-n)}{2J(J+1)}\right]^{1/2}$	$\left[\frac{(J-n+1)(J-n)}{(2J+2)(2J+1)}\right]^{1/2}$
$\langle \Sigma_{(0)} \|$ $(K=n)$	$\left[\frac{(J+n)(J-n)}{J(2J+1)}\right]^{1/2}$	$\frac{-n}{[J(J+1)]^{1/2}}$	$-\left[\frac{(J+n+1)(J-n+1)}{(J+1)(2J+1)}\right]^{1/2}$
$\langle \Pi_{(-1)} \|$ $(K=n-1)$	$\left[\frac{(J-n)(J-n+1)}{2J(2J+1)}\right]^{1/2}$	$-\left[\frac{(J+n)(J-n+1)}{2J(J+1)}\right]^{1/2}$	$\left[\frac{(J+n)(J+n+1)}{(2J+2)(2J+1)}\right]^{1/2}$

Only the same subspecies of clusters should be coupled by a T_d or O_h symmetric Hamiltonian.

The resulting matrices are given in Tables IV and V for three and fourfold clusters, respectively. A continued matrix chain describes one particular subspecies of clusters (c_3) or (c_4), respectively, depending on the chosen value of n. For each J there are three different threefold chains: $n=J+1, J-2, J-5, \ldots$; $n=J, J-3, J-6, \ldots$; $n=J-1, J-4, J-7, \ldots$; and four different continued fourfold chains: $n=J+1, J-3, J-7, \ldots$; $n=J, J-4, J-8, \ldots$; $n=J-1, J-5, J-7, \ldots$; $n=J-2, J-6, J-10, \ldots$.

In the following section an approximate spectrum of the centrifugal Hamiltonian ($g\neq 0$, $B\zeta=0$) is derived using perturbation theory on the BOA representation. The results indicate that a numerical procedure which just diagonalizes a truncated chain of matrices, i.e., just a few of the highest (n) blocks, might be very useful, particularly for $B\zeta\neq 0$. The BOA representations of the centrifugal part are much simpler than their WC counterparts in Table I. While the Coriolis part is not diagonal in the BOA representation, it is a simple tridiagonal form which mixes only states of the same (n), as shown in Table VI. In any case, either cluster basis represents a tremendous simplification over the full $(6J+3)\times(6J+3)$ matrix diagonalization which has been required in the past for each J. We now compare BOA perturbation results with those of the full diagonalization for the T_{1u} spectrum with $J=60$ and $B\zeta=0$.

IV. CORIOLIS-FREE SPECTRUM OF $[2\times 2]^4$ CENTRIFUGAL OPERATOR

We now derive approximate formulas for a T_{1u} or $T_2(\nu_3)$ spectrum of the centrifugal Hamiltonian operator in Eq. (19), and consider $J=60$ as an example. Such a potentially complex spectrum is made quite simple in the cluster basis by our ability to break it into several pieces which can be treated separately.

In order to see what the pieces of a T_{1u} spectrum will be and how they fit together, one may begin by looking at a semiclassical matrix. Consider a (3×3) matrix,

$$H^{[2\times 2]^4}_{\text{semiclassical}} = \begin{array}{c} \begin{array}{ccc} \langle\phi^1_1| & \langle\phi^1_0| & \langle\phi^1_{-1}| \end{array} \\ \begin{pmatrix} \sqrt{6}\,T^2_0 & -2\sqrt{2}\,T^2_{-1} & 5T^2_2+T^2_{-2} \\ 2\sqrt{2}\,T^2_1 & -2\sqrt{6}\,T^2_0 & 2\sqrt{2}\,T^2_{-1} \\ 5T^2_{-2}+T^2_2 & -2\sqrt{2}\,T^2_1 & \sqrt{6}\,T^2_0 \end{pmatrix} \end{array}, \quad (23)$$

which is derived from Eq. (19b) by treating only the vibrational part according to quantum rules. Then by replacing each rotational tensor T^k_q by an equivalent spherical harmonic, i.e., by letting

$$\begin{aligned} T^2_{\pm 2} &\to (x \pm iy)^2 , \\ T^2_{\pm 1} &\to \mp 2z(x \pm iy) , \\ T^2_0 &\to \tfrac{2}{3}(2z^2 - x^2 - y^2) , \end{aligned} \quad (24)$$

one obtains the following matrix:

TABLE IV. Upper diagonal of threefold centrifugal matrix in BOA cluster basis [$g=(12/7)^{1/2}$ is chosen].[a]

n			$n-3$		
$\|\Pi_+\rangle$	$\|\Sigma_0\rangle$	$\|\Pi_-\rangle$	$\|\Pi_+\rangle$	$\|\Sigma_0\rangle$	$\|\Pi_-\rangle$
0	0	0			
$-\frac{10}{3}W^J_2(n+3)$	0	0			
$\frac{10}{3}\sqrt{2}\,W^J_1(n+2)$	$\frac{10}{3}W^J_2(n+2)$	0			
$-\frac{2}{3}W^J_0(n+1)$	$-\frac{4}{3}\sqrt{2}\,W^J_1(n+1)$	$-\frac{2}{3}W^J_2(n+1)$	0	0	0
	$\frac{4}{3}W^J_0(n)$	$\frac{4}{3}\sqrt{2}\,W^J_1(n)$	$-\frac{10}{3}W^J_2(n)$	0	0
		$-\frac{2}{3}W^J_0(n-1)$	$\frac{10}{3}\sqrt{2}\,W^J_1(n-1)$	$\frac{10}{3}W^J_2(n-1)$	0
			$-\frac{2}{3}W^J_0(n-2)$	$-\frac{4}{3}\sqrt{2}\,W^J_1(n-2)$	$-\frac{2}{3}W^J_2(n-2)$
				$\frac{4}{3}W^J_0(n-3)$	$\frac{4}{3}\sqrt{2}\,W^J_1(n-3)$
					$-\frac{2}{3}W^J_0(n-4)$

[a]Values of components are given by

$$W^J_0(n)=2[3n^2-J(J+1)], \quad W^J_1(n)=(2n-1)[(J+n)(J-n+1)]^{1/2}, \quad W^J_2(n)=[(J+n)(J+n-1)(J-n+2)(J-n+1)]^{1/2}.$$

$$H^{[2\times2]^4}_{\text{semiclassical}} = \begin{pmatrix} & |\phi^1_1\rangle & |\phi^1_0\rangle & |\phi^1_{-1}\rangle \\ & 2(2z^2-x^2-y^2) & -4\sqrt{2}\,z(x-iy) & 5(x+iy)^2+(x-iy)^2 \\ & -4\sqrt{2}\,z(x+iy) & -4(2z^2-x^2-y^2) & 4\sqrt{2}\,z(x-iy) \\ & 5(x-iy)^2+(x+iy)^2 & 4\sqrt{2}\,z(x+iy) & 2(2z^2-x^2-y^2) \end{pmatrix}. \tag{25}$$

Finally, it is possible to find approximately the relative energy of the high (n) threefold or fourfold clusters by setting (x, y, z) equal to a threefold axis $(1/\sqrt{3}, 1/\sqrt{3}, 1/\sqrt{3})$ or a fourfold axis $(1, 0, 0)$, respectively. The latter gives eigenvalues 4, 4, and -8 directly, while the former after diagonalization gives eigenvalues $-8/3$, $-8/3$, and $16/3$. More interesting, however, are the crossover points which one finds by using a twofold axis such as $(1/\sqrt{2}, 1/\sqrt{2}, 0)$. The twofold eigenvalues work out to be 4, 2, and -6. By plotting these eigenvalues as shown in Fig. 2, one may deduce the overall character of the T_{1u} spectrum. At the bottom ($H=-8$) the fourfold clusters begin and run until the crossover point at ($H=-6$). These clusters will be called the fourfold "Σ clusters" since the eigenvalue ($H=-8$) belongs to eigenvector $|\Phi^1_0\rangle$ of $H^{[2\ 2]}$ in Eq. (25). Between ($H=-6$) and ($H=2$) there is a long region which is inhabited by threefold "Π clusters," and which borders the fourfold Π cluster region. The spectrum is completed by threefold Σ clusters on top. The threefold Π cluster "starting point" is at ($H=-8/3$) while the threefold Σ clusters start at ($H=16/3$). Interestingly, the fourfold Π cluster starting point lies right on top of the crossover point at ($H=4$) between threefold Σ and fourfold Π. This coincidence feature has not been seen in the other cluster analyses done so far.

Now the details of the spectrum inside each region are derived and compared to the exact full diagonalization using Krohn's[21] codes for $J=60$.

A. Threefold and fourfold Σ clusters

The center component of each (n) block in Tables IV and V gives the corresponding zeroth-order BOA Σ level. As n decreases the offdiagonal $\Sigma \rightleftharpoons \Pi$ perturbations increase significantly, so at least a first order perturbation calculation is needed to obtain useful results. For the threefold Σ clusters one may use the following,

$$\frac{W^{(1)}(\Sigma,\ \text{threefold},\ n)}{g\sqrt{7/12}} = \tfrac{4}{3}W_0(n) + \frac{16}{3}\left\{\frac{[W_1(n+1)]^2}{2W_0(n)+W_0(n+1)} + \frac{[W_1(n)]^2}{2W_0(n)+W_0(n-1)}\right\}, \tag{26a}$$

while for fourfold Σ clusters the following is appropriate,

$$\frac{W^{(1)}(\Sigma,\ \text{fourfold},\ n)}{g\sqrt{7/12}} = -2W_0(n) - 8\left\{\frac{[W_1(n+1)]^2}{2W_0(n)+W_0(n+1)} + \frac{[W_1(n)]^2}{2W_0(n)+W_0(n-1)}\right\}. \tag{26b}$$

In Table VII several zeroth-order and first-order eigenvalues are compared with the exact results. As one might expect the first-order perturbation over corrects slightly. Presumably, second-order corrections would bring it back, but we saw no point in obtaining greater precision here.

It is important to see that the qualitative predictions are right. The beginning Σ clusters have $n=60$. For the fourfold case we have $60=0$ mod4 so a $(0_4)=A_1+T_1+E$ cluster is expected. This is right according to the exact results as shown in Fig. 3. For the threefold case one starts with a $(0_3)=A_1+T_1+T_2+A_2$ cluster since $60=0$ mod3. Identifying the outside threefold cluster level ($W=19.26$ in Table VII) with the corresponding eigenvalue ($H=16/3$) of the semiclassical ma-

TABLE V. Upper diagonal of fourfold centrifugal matrix in BOA cluster basis [$g=(12/7)^{1/2}$ is chosen].[a]

n			$n-4$		
$\|\Pi_+\rangle$	$\|\Sigma_0\rangle$	$\|\Pi_-\rangle$	$\|\Pi_+\rangle$	$\|\Sigma_0\rangle$	$\|\Pi_-\rangle$
0	0	0			
0	0	0			
$5W^J_2(n+3)$	0	0			
$W^J_0(n+1)$	$2\sqrt{2}\,W^J_1(n+1)$	$W^J_2(n+1)$	0	0	0
	$-2W^J_0(n)$	$-2\sqrt{2}\,W^J_1(n)$	0	0	0
		$W^J_0(n-1)$	$5W^J_2(n-1)$	0	0
			$W^J_0(n-3)$	$2\sqrt{2}\,W^J_1(n-3)$	$W^J_2(n-3)$
				$-2W^J_0(n-4)$	$-2\sqrt{2}\,W^J_1(n-4)$
					$W^J_0(n-5)$

[a]Values of components are given in Table IV.

TABLE VI. Upper diagonal of $2(J\cdot l)$ matrix in BOA cluster basis.

	n	
$\|\Pi_+\rangle$	$\|\Sigma_0\rangle$	$\|\Pi_-\rangle$
$2(n+1)$	$[2(J+n+1)(J-n)]^{1/2}$	0
	0	$[2(J-n+1)(J+n)]^{1/2}$
		$-2(n-1)$

trix $H^{[2\times2]}$ [Eq. (25)] one may predict other singular points by multiplying the other H values by $r=19.26(3/16)$. One predicts a crossover of the fourfold Σ to the threefold Π at $(H=-6)=-21.66$ which is seen to be exactly right according to Fig. 3. The same goes for the threefold Π to fourfold Π crossover at $r(H=2)=7.22$. However, the fourfold Π to threefold Σ crossover predicted a $r(H=4)=14.44$ seems to be about 2% low. One might have expected some anomaly at this point given the coincidence between twofold and fourfold H values.

B. Threefold Π clusters

The threefold Π clusters have extraordinarily large mixing between states $|\Pi_- n\rangle$ and $|\Pi_+ n-3\rangle$ due to the matrix element $[10\sqrt{2}\,W_1(n-1)/3]$. Hence, the diagonal or zeroth-order BOA (Π) values will be split apart widely in a way that reminds one of the behavior of three threefold E cluster patterns in Ref. 9. By solving for the eigenvalues of the matrix,

$$S=-2/3\begin{array}{c} \begin{matrix} |\Pi_- n\rangle & |\Pi_+ n-3\rangle \end{matrix} \\ \begin{pmatrix} W_0(n-1) & -5\sqrt{2}\,W_1(n-1) \\ -5\sqrt{2}\,W_1(n-1) & W_0(n-2) \end{pmatrix} \end{array}, \quad (27)$$

one obtains the first-order Π eigenvalue formula,

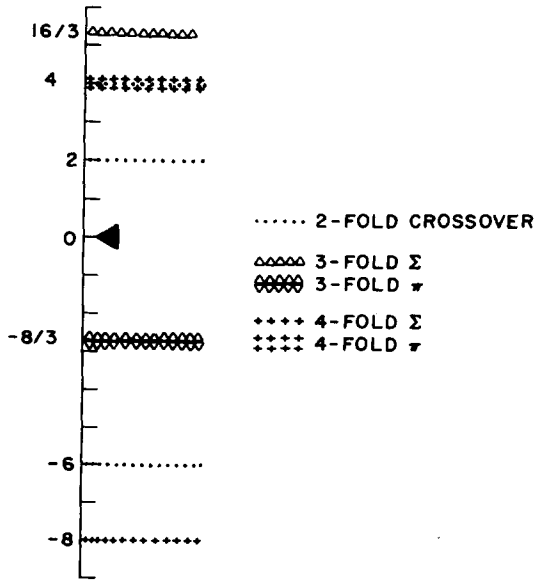

FIG. 2. Semiclassical $[2\times2]^4$ centrifugal (T_1) eigenvalues for zero Coriolis parameter ($B\zeta=0$).

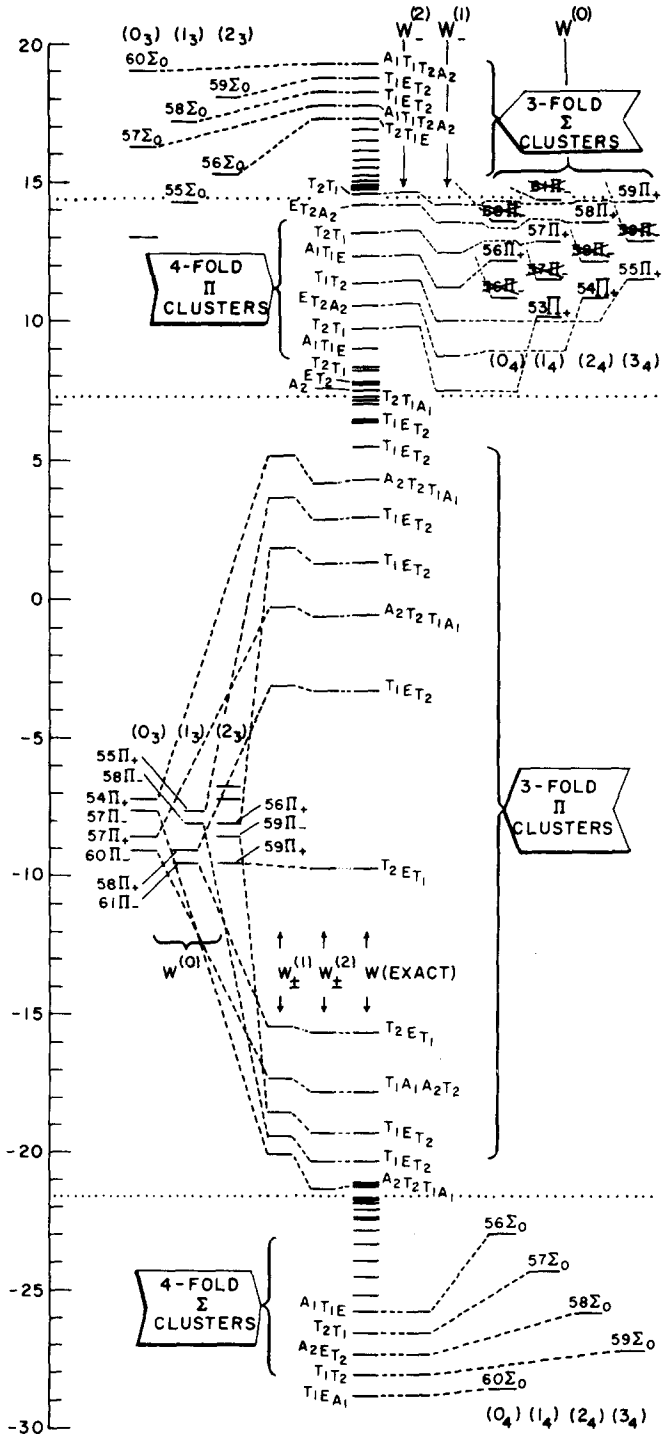

FIG. 3. $(J=60,\ T_1)$ $[2\times2]^4$ centrifugal eigenvalues for zero Coriolis parameter ($B\zeta=0$). Various approximations are compared with the exact eigenvalues.

$$W_\pm^{(1)}(n)=-\tfrac{8}{3}(n-1)(n-2)+\tfrac{4}{3}(J-n+2)(J+n-1)-2 \pm\tfrac{5}{3}(2n-3)[8(J-n+2)(J+n-1)+9/50]^{1/2}, \quad (28)$$

where we have set $g=(12/7)^{1/2}$.

Note, however, that the state $|\Pi_+ n=J-1\rangle$, which in the present example is $|\Pi_+ n=59\rangle$, has no strong coupling partner. (It would have to be $|\Pi_- n=62\rangle$ which doesn't exist for $J=60$.) Since $n=59=2$ mod3, we have a "lone" $(2_3)=T_1+E+T_2$ cluster in the middle of the threefold

TABLE VII. Examples of $(J=60)$ Σ cluster energies. Comparison is made between approximate values [Eq. (26) and Tables IV and V] and exact computer produced values for $g=10^{-3}(12/7)^{1/2}$.

	$W^{(0)}$	$W^{(1)}$	W(exact)
	(a) Threefold clusters		
$n=60$	19.04	19.255	19.2567
59	18.09	18.741	18.7407
58	17.15	18.253	18.247
57	16.25	17.811	17.777
56	15.33	17.361	17.331
	(b) Fourfold clusters		
$n=60$	−28.560	−28.883	−28.881
59	−27.132	−28.112	−28.095
58	−25.728	−27.379	−27.331

$(J=60)$ Π pattern. It is perturbed only slightly by the threefold $|\Sigma n=J-1\rangle$ state.

The first "split pair" of threefold Π's in $J=60$ involves a combination of $|\Pi_- n=61\rangle$ and $|\Pi_+ n=58\rangle$ states, both of which belong to $(1_3)=T_1+E+T_2$ clusters according to Eq. (2). For simplicity of calculation we will assume that all split-pair eigenvectors are approximately,

$$|n_+\rangle \cong (|\Pi_- n\rangle + |\Pi_+ n-3\rangle)/\sqrt{2}\ ,$$
$$|n_-\rangle \cong (|\Pi_- n\rangle - |\Pi_+ n-3\rangle)/\sqrt{2}\ , \tag{29}$$

which is true as long as the diagonal components of S [Eq. (27)] are nearly equal. This allows one to make simpler Σ perturbation formulas. The second-order results (these are actually *first*-order perturbations) are as follows:

$$W_\pm^{(2)}(n) = W_\pm^{(1)}(n) + \frac{|\langle \Sigma_0 n|H|n_\pm\rangle|^2}{W_\pm^{(1)}(n)-(4/3)W_0(n)} + \frac{|\langle \Sigma_0 n-3|H|n_\pm\rangle|^2}{W_\pm^{(1)}(n)-(4/3)W_0(n-3)}$$
$$= W_\pm^{(1)}(n) + \frac{|(4\sqrt{2}/3)W_1(n) \mp (10/3)W_2(n)|^2}{2[W_\pm^{(1)}(n)-(4/3)W_0(n)]} + \frac{|(10/3)W_2(n-1) \mp (4\sqrt{2}/3)W_1(n-2)|^2}{2[W_\pm^{(1)}(n)-(4/3)W_0(n-3)]}\ , \tag{30}$$

where again we set $g=(12/7)^{1/2}$. The first and second-order results are compared with the exact eigenvalues in Table VIII and in Fig. 3.

C. Fourfold Π clusters

The behavior of the fourfold Π clusters can be explained in terms of the mixing between $|\Pi_- n\rangle$ and $|\Pi_+ n-4\rangle$ states due to the matrix element $[5W_2(n-1)]$. By solving for the eigenvalues of the matrix,

$$S = \begin{array}{c} \begin{matrix} |\Pi_- n\rangle & |\Pi_+ n-4\rangle \end{matrix} \\ \begin{pmatrix} W_0(n-1) & 5W_2(n-1) \\ 5W_2(n-1) & W_0(n-3) \end{pmatrix} \end{array}\ , \tag{31}$$

one obtains the first order Π eigenvalue formula,

$$W_\pm^{(1)}(n) = 6(n^2-4n+5) - 2J(J+1) \pm \{144(n-2)^2 + 25[(J+n+1)(J-n+3)(J^2-(n-2)^2)]\}^{1/2}\ , \tag{32}$$

where $g=(12/7)^{1/2}$.

Note that the states $|\Pi_+ J-1\rangle$ or $|\Pi_+ J-2\rangle$ can have no partners $|\Pi_- J+3\rangle$ or $|\Pi_- J+2\rangle$. Hence in our example for $J=60$ we have two lone clusters for $n=59=3$ mod4 and $n=58=2$ mod4 corresponding to $(3_4)=T_1+T_2$ and $(2_4)=A_2+T_2+E$, respectively. These two clusters can be seen in Fig. 3 very close to the threefold Σ crossover point. They are only very slightly perturbed by the fourfold $|\Sigma J-1\rangle$ or $|\Sigma J-2\rangle$ states, respectively, as can be seen in Table IX.

The first split pair is the $|\Pi_- J+1\rangle$ and $|\Pi_+ J-3\rangle$. In our example $(J=60)$, both of these states belong to the $(1_4)=T_1+T_2$ cluster according to Eq. (1). Unlike the threefold Π case, we cannot assume an equal mixing of the split states. In fact, we can associate the $|\Pi_- n\rangle$ state with the $W_+^{(1)}(n)$ eigenvalue and the $|\Pi_+ n-4\rangle$ state with the $W_-^{(1)}(n)$ eigenvalue. That is,

$$|n_+\rangle \equiv |\Pi_- n\rangle^{\text{perturbed}} \equiv \mu_+|\Pi_- n\rangle + \nu_+|\Pi_+ n-4\rangle\ ,$$
$$|n_-\rangle \equiv |\Pi_+ n-4\rangle^{\text{perturbed}} \equiv \mu_-|\Pi_- n\rangle + \nu_-|\Pi_+ n-4\rangle\ , \tag{33}$$

where

$$\mu_+ = -\nu_- = x/(x^2+y^2)^{1/2}\ ,$$
$$\nu_+ = \mu_- = y/(x^2+y^2)^{1/2}\ , \tag{34}$$

and where one sees that usually $x \gg y$ according to their definitions:

TABLE VIII. Examples of $(J=60)$ threefold Π cluster energies. Comparison is made between approximate values [see Eqs. (28)–(30) and Table IV] and exact computer produced values for $g=10^{-3}(12/7)^{1/2}$.

"lone state"

$|n=59\ \Pi_+\rangle$: $W^{(0)}=-9.57$ $W^{(1)}=-9.75$ W(exact) $=-9.734$

	$W_\pm^{(1)}$	$W_\pm^{(2)}$	W(exact)
$(n,n-3)=(61,58)$	−3.14	−3.335	−3.330
	−15.43	−15.669	−15.657
(60, 57)	−0.30	−0.687	−0.672
	−17.32	−17.82	−17.787
(59, 56)	1.85	1.28	1.312
	−18.55	−19.33	−19.25
(58, 55)	3.63	2.85	2.93
	−19.41	−20.50	−20.34
(57, 54)	5.16	4.14	4.28
	−20.04	−21.44	−21.22[a]

[a]Last threefold cluster.

TABLE IX. Examples of ($J=60$) fourfold Π cluster energies. Comparison is made between approximate values [see Eqs. (32)–(36) and Table V] and exact computer produced values for $g=10^{-3}\,(12/7)^{1/2}$.

n	W^0	W^1	W^2	W(exact)
$\lvert \Pi_+ 59\rangle$	14.28	14.61		14.528
$\lvert \Pi_+ 58\rangle$	13.57	14.23		14.131
$\lvert \Pi_- 61\rangle$	14.28	14.67	14.84	•••
$\lvert \Pi_+ 57\rangle$	12.86	12.47	13.30	13.168
$\lvert \Pi_- 60\rangle$	13.57	14.48	15.06	•••
$\lvert \Pi_+ 56\rangle$	12.17	11.26	12.36	12.244
$\lvert \Pi_- 59\rangle$	12.86	14.33	15.29	•••
$\lvert \Pi_+ 55\rangle$	11.50	10.03	11.48	11.353
$\lvert \Pi_- 58\rangle$	12.17	14.19	15.49	•••
$\lvert \Pi_+ 54\rangle$	10.83	8.81	10.62	10.504
$\lvert \Pi_- 57\rangle$	11.50	14.07	15.70	•••
$\lvert \Pi_+ 53\rangle$	10.18	7.60	9.85	9.704
$\lvert \Pi_- 56\rangle$	10.83	13.95	15.89	•••
$\lvert \Pi_+ 52\rangle$	9.53	6.42	9.15	8.961

$$y=-12(n-2)+\{144(n-2)^2 + 25\{(J+n+1)(J-n+3)[J^2-(n-2)^2]\}\}^{1/2}\,, \quad (35)$$

$$x=5[(J+n-1)(J+n-2)(J-n+3)(J-n+2)]^{1/2}\,.$$

As in the threefold case, we can now use perturbation theory to calculate the second-order results as follows:

$$W_\pm^{(2)}(n)=W_\pm^{(1)}(n)+\frac{|\langle\Sigma n|H|n_\pm\rangle|^2}{W_\pm^{(1)}(n)+2W_0(n)}+\frac{|\langle\Sigma n-4|H|n_\pm\rangle|^2}{W_\pm^{(1)}(n)+2W_0(n-4)}$$

$$=W_\pm^{(1)}(n)+\frac{8|\mu_\pm W_1(n)|^2}{W_\pm^{(1)}(n)+2W_0(n)}+\frac{8|\nu_\pm W_1(n-3)|^2}{W_\pm^{(1)}(n)+2W_0(n-4)} \quad (36)$$

where again we set $g=(12/7)^{1/2}$. The first and second-order results are compared with the exact eigenvalues in Table IX. Note that for perturbed $\lvert \Pi_+ n-4\rangle$ states the first and second-order corrections to the energy nearly cancel each other so that,

$$W_-^{(2)}(n)\simeq W_0(n-3)\,. \quad (37)$$

Thus the zeroth-order energies in Fig. 3 are very nearly correct. Furthermore, the energies for the perturbed $\lvert \Pi_- n\rangle$ states are raised beyond the crossover for threefold Σ state and hence are not good cluster states. We may therefore ignore the $\lvert \Pi_- n\rangle$ states (they are crossed out in Fig. 3) and explain the fourfold Π clusters *entirely* in terms of the $\lvert \Pi_+ n-4\rangle$ states. Thus none of the fourfold Π clusters occur in pairs as they did for the threefold Π clusters.

V. WC-BOA CLUSTERS AND LEVEL CORRELATIONS

It is interesting to vary $B\zeta$ for constant g to test the validity of our cluster approximations for the octahedral level splittings of ν_3 excited states (T_2 and T_{1u} modes) with high angular momentum. Such splittings reveal striking and complicated level or cluster crossings. For each J, the separate branches of good $N=J+1$, J, and $J-1$ will be rearranged to form, as $B\zeta$ decreases, the Σ and Π patterns of Sec. IV.

This rearrangement is clearly shown in Fig. 4 where H_M has been diagonalized in a $J=60$ cluster basis for varying $B\zeta$ and $g=\sqrt{12/7}\,(0.001)$. Only the 3×3 diagonal submatrices (for which $\Delta n=0$) of the octahedral ten-

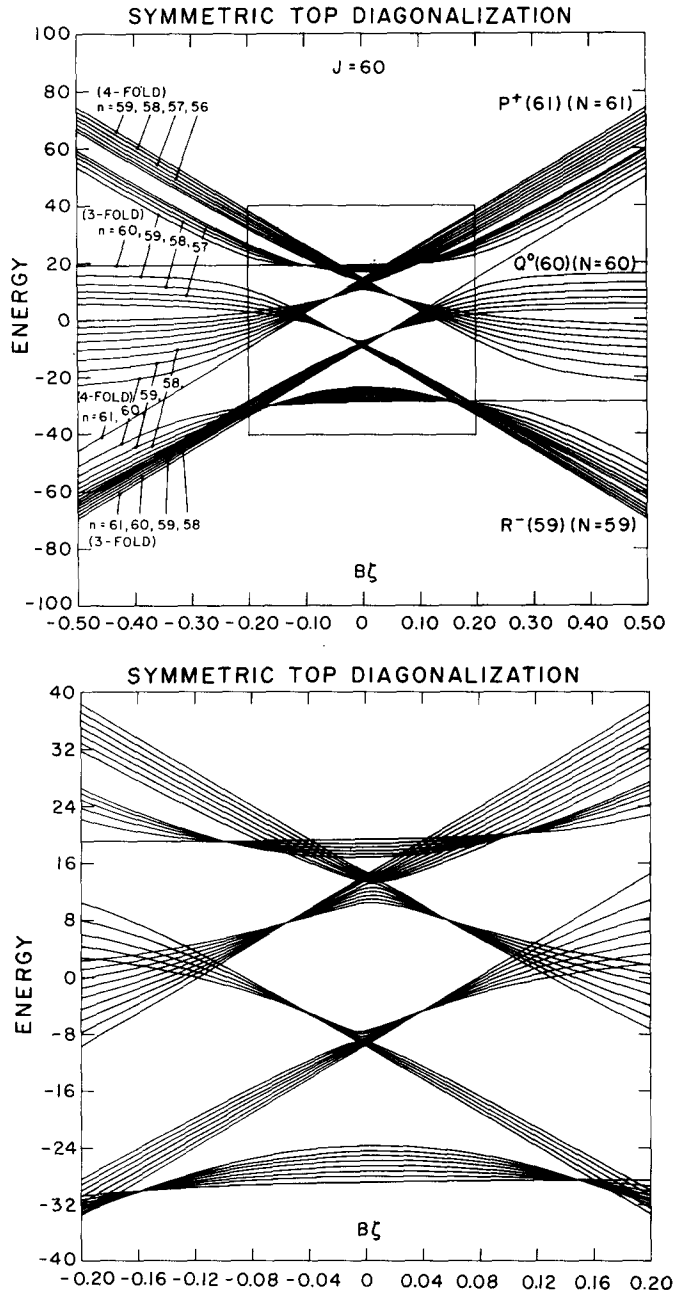

FIG. 4. (a) Threefold and fourfold cluster splitting of the $J=60$ ν_3 excited state found by diagonalizing H_M[Eq. (3a)] in a cluster basis. Only the 3×3 submatrices of $[\bar{V}^2(\text{rot})\times\bar{V}(\text{vib})]^4$ for which $\Delta n=0$ in Tables I, II or IV, V have been included in diagonalization. Here $B\zeta$ is varied and $g=(12/7)^{1/2}(0.001)$. On the right and left where $|B\zeta|\gg g$, the WC approximation is valid, and we have labeled the clusters for the P, Q, and R branches. (b) Expanded view of (a) in the region where the BOA approximation is valid.

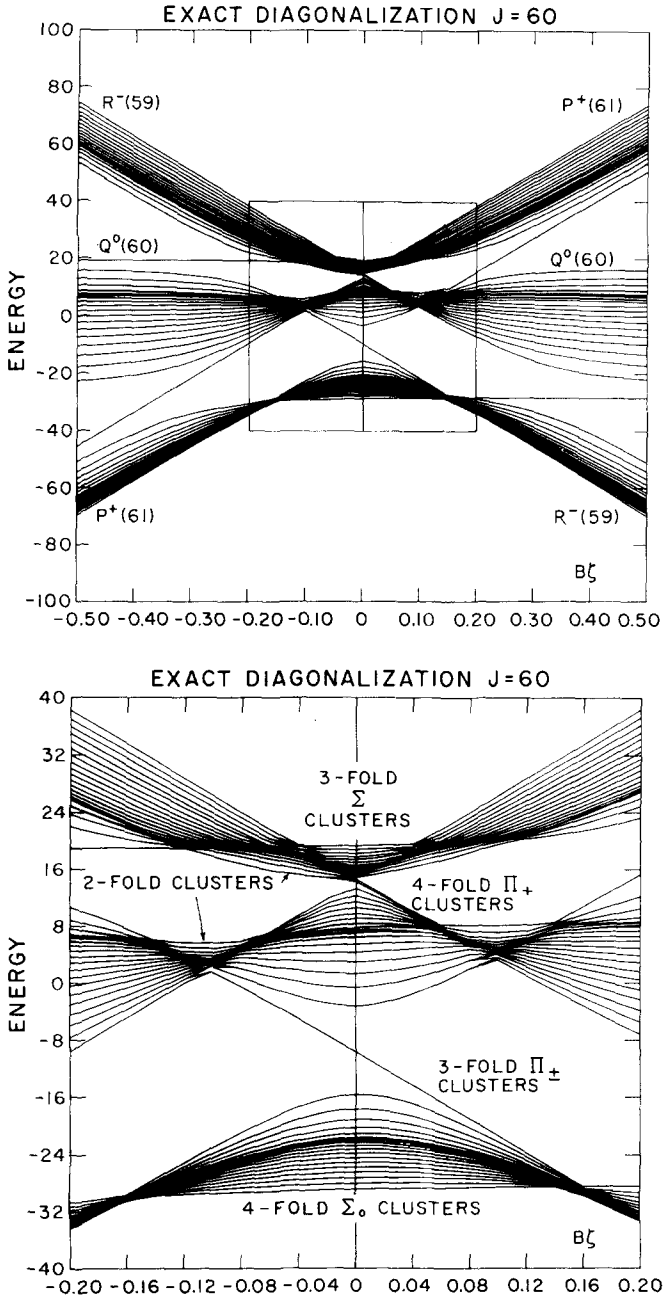

FIG. 5. (a) Octahedral splitting of the $J=60$ ν_3 excited state found by diagonalizing H_M [Eq. (3a)] in a full octahedral basis. Again, $B\zeta$ is varied and $g=(12/7)^{1/2}(0.001)$. (b) Expanded view of (a). (Compare the $B\zeta=0$ values with Fig. 3.)

sor (see Tables I, II, and IV, V) have been used in the diagonalization. (The diagonal submatrices in Tables I and II are in the WC cluster basis, while the diagonal submatrices in Tables IV and V are in the BOA cluster basis. Diagonalizing H_M in either $\Delta n=0$ cluster subbasis leads to the same results.) One can see in Fig. 4 that the threefold and fourfold Π_+ and Π_- clusters are not separated as much as they should be at $B\zeta=0$. (Recall Fig. 3.) This is because the symmetric top approximation ignores the $\Delta n=\pm 3$ and $\Delta n=\pm 4$ interactions.

In Fig. 5 we show the octahedral splitting of the $J=60$ ν_3 excited state where we have diagonalized H_M in the full octahedral basis. We see that the clustering behavior of the octahedral terms for varying $B\zeta$ in Fig. 5 is qualitatively reproduced by Fig. 4. Indeed, on the far right and left where $|B\zeta| \gg g$, the P, Q, and R clusters in Fig. 4a are quite accurate. This is the region where the "dominant approximation" is valid so that the WC diagonal submatrices in Table I give accurate results. Also, for $|B\zeta| \sim 0$ the Σ clusters in Fig. 4b are quite accurate. Again, this is because the BOA diagonal submatrices in Tables IV and V correctly describe Σ clustering as shown in Sec. IV.

An interesting feature of Fig. 5 which is qualitatively reproduced in Fig. 4 is the convergence of threefold and fourfold clusters for each of the R, Q, and P branches. These are extremely complicated regions where the clusters in each P, Q, and R branch recombine to form Σ and Π threefold and fourfold clusters, and they can only be explained by including the off-diagonal submatrices in Tables I, II or IV, V where $\Delta n=\pm 3$ or ± 4 for threefold or fourfold clusters, respectively. The occurrence of these convergences in an actual molecule giving rise to such a remarkable spectral "signature" would certainly help in making line assignments. So also would the "lone" Π_+ threefold cluster which has an energy which varies linearly with $B\zeta$!

The convergence of the three- and fourfold clusters occurs in an intermediate region where the tensor splitting is approximately equal to the Coriolis splitting. The tensor splitting may be found in the WC approximation from the diagonal $N=J+1$ matrix element in Table I. Thus, in the cluster crossing region we have

$$g(7/12)^{1/2}\{[6(J+2)(J+1)J(J-1)-10n^2(6J^2+6J-5) + 70n^4]/(2J+2)(2J+1)\} \sim 2B\zeta J \,. \tag{38}$$

For the highest cluster ($n=J$) and for large J we have

$$4g(7/12)^{1/2}J^2 \sim 2B\zeta J \,,$$

or

$$B\zeta \sim 2g(7/12)^{1/2}J \,. \tag{39}$$

For $g=(12/7)^{1/2}(0.001)$ and $J=60$ as in Figs. 4 and 5, the intermediate region occurs for $B\zeta \sim 0.12$ as shown. Methane (CH_4), for example, would fall in this region at an angular momentum $J \sim 48$ which is too high to be observed at room temperature because of the Boltzmann factor. We should emphasize that, although we are unaware of any T_2 or T_{1u} tetrahedral or octahedral vibrational spectra belonging to the intermediate or BOA regions of Figs. 4b and 5b, there is nothing "unphysical" about them. Furthermore, it is likely that the parameters for triply degenerate vibrational modes for overtones or combination tones will lie within these regions.

Some extraordinary features in the BOA region have been found by plotting the graphs in color. By assigning three primary colors red, green, and violet to the three types A, E, and F of tetrahedral species, one can identify the chromatic mixtures of colors associated with various kinds of clusters. Close examination of the cluster intersections reveals beautiful interaction effects between primary species wherein equivalent types tend to "repel" each other. Furthermore, a heretofore

unobserved type of "giant" cluster $(A_1+E+F_1+2F_2)$ and $(A_2+E+2F_1+F_2)$ is seen for intermediate values of $B\zeta$, i.e., for $0.02<|B\zeta|<0.16$ when $g=0.001\sqrt{12/7}$ (see Fig. 5b). As shown in Ref. 4 these are *twofold clusters*! Normally, twofold axes are not stable rotation axes, and therefore the energy levels corresponding to twofold rotation do not cluster. In the regions of high $|B\zeta|$ (see Fig. 5a) and also at $(B\zeta=0)$ (see Fig. 3) unclustered twofold energy levels serve as "boundaries" between regions of three- and fourfold clusters. However, in the intermediate regions $(0.02<|B\zeta|<0.16$; see Fig. 5b) it appears that the extreme twofold clusters are extensions of the boundaries between three- and fourfold clusters on either side. Also, it appears that the boundaries of twofold cluster regions are extensions of extreme three- and fourfold cluster trajectories. In fact, the boundaries are seen to be the eigenvalues for $n=J+1$, J, and $J-1$ of the (3×3) submatrices of H_M [Eq. (3a)] computed using Tables IV, V and VI. The $n=59$, 60, and 61 trajectories for three- and fourfold cases are plotted in Fig. 4. Comparison with Fig. 5 shows that they are indeed boundaries of different cluster regions including those of the extraordinary twofold clusters.

[1]A. V. Novak and J. L. Lyman, J. Quant. Spectrosc. Radia. Transfer **15**, 945 (1975).

[2]*Laser Spectroscopy* III, edited by J. L. Hall and J. L. Carlsten (Springer, New York, 1977).

[3]W. G. Harter and C. W. Patterson, Phys. Rev. Lett. **36**, 224 (1977).

[4]W. G. Harter and C. W. Patterson, J. Chem. Phys. **66**, 4872 (1977).

[5]C. W. Patterson and W. G. Harter, J. Chem. Phys. **66**, 4886 (1977).

[6]W. G. Harter and C. W. Patterson, *Quantum Chemistry Symposium* No. 11, Int. J. Quantum. Chem. **S11**, 445 (1977).

[7]W. G. Harter, C. W. Patterson, and F. daPaixao, Rev. Mod. Phys. **50**, 37 (1978).

[8]H. W. Galbraith, C. W. Patterson, B. J. Krohn, and W. G. Harter, J. Mol. Spectrosc. (in press).

[9]W. G. Harter, H. W. Galbraith, and C. W. Patterson, J. Chem. Phys. **69**, 4888 (1978), preceding article.

[10]E. K. Plyler, E. D. Tidwell, and L. R. Blaine, J. Res. Natl. Bur. Stand. Sect. A **64**, 201 (1960).

[11]J. D. Louck, Diss. Abstr. **19**, 840 (1958); K. T. Hecht, J. Mol. Spectrosc. **5**, 355 (1960); J. Moret-Bailly, J. Mol. Spectrosc. **15**, 344 (1965).

[12]H. A. Jahn, Proc. Roy. Soc. A **168**, 469, 495 (1938).

[13]E. D. Hinkley, and P. L. Kelley, Science, **171**, 635 (1971).

[14]J. P. Aldridge, H. Filip, M. Flicker, R. F. Holland, R. S. McDowell, N. G. Nereson, and K. Fox, J. Mol. Spectrosc. **58**, 165 (1975).

[15]R. S. McDowell, in *Laser Spectroscopy* III, edited by J. L. Hall and J. L. Carlsten (Springer, New York, 1977), p. 102.

[16]K. Fox, H. W. Galbraith, B. J. Krohn, and J. D. Louck, Phys. Rev. A **15**, 4, 1363 (1977).

[17]K. R. Lea, M. J. Leask, and W. P. Wolf, J. Phys. Chem. **23**, 1381 (1962).

[18]A. J. Dorney and J. K. G. Watson, J. Mol. Spectrosc. **42**, 1 (1972).

[19](a) R. S. McDowell, H. W. Galbraith, B. J. Krohn, and C. D. Cantrell, Opt. Commun. **17**, 178 (1976); (b) H. W. Galbraith and R. S. McDowell (unpublished); (c) K. Fox, J. Chem. Phys. (in press).

[20]U. Fano, Phys. Rev. A **2**, 353 (1970).

[21]B. J. Krohn, Los Alamos Report LA-6554-MS, Los Alamos, New Mexico.